Chinese Chemical Letters 31 (2020) 2109–2114

Contents lists available at ScienceDirect

Chinese Chemical Letters

journal homepage: www.elsevier.com/locate/cclet

Communication

High ammonia sensitive ability of novel $Cu_{12}Sb_4S_{13}$ quantum dots@reduced graphene oxide nanosheet composites at room temperature

Yueli Liu[a], Binghua Sang[a], Haoran Wang[a], Zijing Wu[a], Yuxuan Wang[a], Ziwei Wang[a], Zhuoyin Peng[c,*], Wen Chen[b,*]

[a] State Key Laboratory of Silicate Materials for Architectures, School of Materials Science and Engineering, Wuhan University of Technology, Wuhan 430070, China
[b] State Key Laboratory of Advanced Technology for Materials Synthesis and Processing, School of Materials Science and Engineering, Wuhan University of Technology, Wuhan 430070, China
[c] The Key Laboratory of Efficient & Clean Energy Utilization, School of Energy and Power Engineering, Changsha University of Science and Technology, Changsha 410111, China

ARTICLE INFO

Article history:
Received 10 October 2019
Received in revised form 4 December 2019
Accepted 24 December 2019
Available online 24 December 2019

Keywords:
$Cu_{12}Sb_4S_{13}$ quantum dots@rGO nanosheet
Composites
NH_3
Room temperature
Gas response

ABSTRACT

In the work, rGO nanosheet is synthesized using the typical Hummer's method, then $Cu_{12}Sb_4S_{13}$ quantum dots@rGO composites are prepared by solvent thermal method, and $Cu_{12}Sb_4S_{13}$ quantum dots with the average size of 5 nm are densely distributed on the surface of rGO sheet. NH_3 gas response of $Cu_{12}Sb_4S_{13}$ quantum dots@rGO nanosheet composites at room temperature of 25 °C is enhanced compared with the pure $Cu_{12}Sb_4S_{13}$ quantum dots and rGO nanosheet, and the composites possess an excellent stability during the humidity range of 45%–80% with a low detection limit of 1 ppm, which is related with the intrinsic hydrophobicity characteristic of $Cu_{12}Sb_4S_{13}$ quantum dots. It also proves that $Cu_{12}Sb_4S_{13}$ quantum dots@rGO nanosheet composites have a quite high selectivity towards ammonia compared with ethanol, methanol, acetone, toluene, hydrogen sulfide and nitrogen dioxide at room temperature. The gas sensing mechanism of the composites is discussed primarily.

In recent decades, industrialized urbanization has developed rapidly and led to a large number of atmospheric pollution caused by industrial exhaust gas, which seriously influences people's life [1–3]. Inside them, ammonia (NH_3) is harmful to the human health [4,5]. Therefore, it is quite important to apply gas sensors with high performance to realize the accurate detection for the purpose of reducing losses.

As the key factor of gas sensors, gas sensing material directly determines the sensitivity, selectivity, response time and stability of gas sensors. At present, metal oxide materials are widely used, such as TiO_2 [6], V_2O_5 [7], SnO_2 [8], ZnO [9], MoO_3 [10], WO_3 [11] and so forth. However, metal oxides possess the shortcoming of high working temperature and low selectivity. Therefore, it is urgent to explore novel gas sensing materials at room temperature. Quantum dots have drawn extensive attention for gas sensing due to the special characters, such as large specific surface area [12], rich surface defect [13] and the size effect in nano-scale [14]. ZnO quantum dots have shown excellent gas response towards 50 ppm H_2S at room temperature [15]. SnO_2 quantum dots possess the maximum response value of 15 to 1 ppm triethylamine [16]. PbSe quantum dots are found to be sensitive and selective to NO_2 with a gas response of 22.3 at 50 ppm and a quick gas response time (7 s) [17]. Recently, $Cu_{12}Sb_4S_{13}$ quantum dots with direct band gap are theoretically considered to be the novel candidate in gas sensing applications, as they are very sensitive to the variation of carrier concentration due to the existence of two non-occupied states of Sb site in the valence band. Moreover, S element is much active in the air, which is beneficial to the adsorption and reaction of gas [18–20]. However, $Cu_{12}Sb_4S_{13}$ quantum dots suffer the shortcoming of the excessive resistance of the gas sensors due to the plenty of grain boundaries.

To solve the above problem, it is found that quantum dots composited with graphene may effectively prevents the aggregation of quantum dots and favor for the fast electron transfer, achieving the excellent gas sensing performance at room temperature [21,22].

* Corresponding authors.
E-mail addresses: joeypengzy@outlook.com (Z. Peng), chenw@whut.edu.cn (W. Chen).

https://doi.org/10.1016/j.cclet.2019.12.030

Cu_2O quantum dots are grow on functionalized graphene, which possess room temperature sensing to H_2S with the fantastic sensitivity (11%) [23]. SnO_2 quantum dots/rGO possesses the great gas sensing behaviors of 89.3% to H_2 and 92.4% to LPG for 500 ppm, respectively [24]. PbS quantum dots/rGO nanocoons show an excellent ammonia sensing performance at room temperature due to the Schottky barrier modulation [25]. Novel $CuSbS_2$ QD/rGO composite possesses superb ammonia detection with ppb level at room temperature, while it suffers the shortcoming of poor stability at high relative humidity over 65% [26]. However, it is still needed to develop the novel gas sensing composite to realize the rapid development of the gas sensors.

In the present work, $Cu_{12}Sb_4S_{13}$ quantum dots@rGO nanosheet composites are prepared by solvent thermal method, and the ammonia gas response at room temperature of 25 °C is firstly reported. It is expected that $Cu_{12}Sb_4S_{13}$ quantum dots@rGO nanosheet composites may have a good gas response and selectivity towards ammonia at room temperature.

Oleylamine (OLA, 80%–90%), Diphenyl ether ($C_{12}H_{10}O$, >99%), N, N-Diphenylthiourea ($C_{13}H_{12}N_2S$, 98%) and Antimony trichloride ($SbCl_3$, 99%) with analytical grade were bought from Aladdin, while Cuprous iodide (CuI, 99%) were purchased from Alfa Aesar. All solvents were bought from Sinopharm Chemical Reagent Co., Ltd. in China. Reduced graphene oxide (rGO) was synthesized by the traditional Hummer's method [25,26]. For the synthesis of $Cu_{12}Sb_4S_{13}$ quantum dots@rGO nanosheet composites by solvent thermal method, 0.0252 g rGO was dissolved in the precursor solution for the synthesis of $Cu_{12}Sb_4S_{13}$ quantum dots, and the synthesis conditions were controlled to be the same as mentioned in the synthesis of $Cu_{12}Sb_4S_{13}$ quantum dots in our group [26–28].

X-ray diffraction patterns of the samples were measured by an X-ray diffractometer (XRD, Pert-Pro, PANalytical, Netherlands) with Cu Kα radiation. Raman spectra were measured by Raman spectroscopy (Raman, Invia, Renishaw, England) with 514.5 nm laser. The microstructures were tested by Field emission scanning electron microscope (FESEM, JSEM-5610LV, Hitachi, Japan) and High resolution transmission electron microscope (HRTEM, JEM-2100 F, JEOL, Japan). Diffuse reflectance infrared Fourier transform spectra were applied by the device (DRIFT, Nicolet 6700, Nicolet, America) with a liquid N_2 cooled MCT detector, and the gas molecules charged into the tiny chamber was regulated by a MFC. The spectral resolution of DRIFT was 4 cm^{-1} while the IR signals were originated from the accumulation of reflectance with 32 scans. Specific surface areas of the samples were measured by nitrogen adsorption at 77 K (Micromeritics Tristar ASAP 2020) by using Brunauer-Emmett-Teller (BET) method.

The sensor devices were fabricated on ceramic tube, $Cu_{12}Sb_4S_{13}$ quantum dots@rGO nanosheet composites were dispersed in deionized water and deposited on the surface of ceramic tube by spin-coating (1000 rpm, 30 s), and then it was dried in the vacuum oven at room temperature to obtain the gas sensors [25,26].

The target gases were obtained by evaporating the certain volume of corresponding liquid on the heater plate of the equipment. When a certain amount of humidity was needed in the gas sensing measurement, the appropriate amount of distilled water was evaporated to calibrate the real-time humidity by the hygrometer. The default relative humidity for the test was well controlled as 45%. The gas sensing measurement of $Cu_{12}Sb_4S_{13}$ quantum dots@rGO nanosheet composites in a static mode was operated with a commercial gas sensing measurement system (WS-30A, Zhengzhou Winsen Technology Corp, Ltd., China). The gas response was defined as R_g/R_a, where R_a and R_g were the average electrical resistance of gas sensor in air and in the target gas, respectively. The response time and recovery time were recorded in real-time by Keithley 4200 with a double-probe device and a mass flow controller (MFC). The definition of gas response and recovery time was the length of periods, in which 90% of the resistance change from the initial to the final state was chosen in this case.

Fig. S1a (Supporting information) shows the XRD pattern of $Cu_{12}Sb_4S_{13}$ quantum dots@rGO nanosheet composites, which indicates the existence of rGO phase in the composites due to the existence of the graphite XRD peaks (JCPDS No. 89-8488). In addition, the X-ray diffraction peaks at 24.21°, 29.98°, 32.43°, 48.05°, 50.22°, 54.60° and 58.91° correspond to the (220), (222), (400), (440), (530), (622) and (631) crystal planes of $Cu_{12}Sb_4S_{13}$ phase (JCPDS No. 74-0270), respectively. Raman spectra of $Cu_{12}Sb_4S_{13}$ quantum dots, rGO nanosheet and $Cu_{12}Sb_4S_{13}$ quantum dots@rGO nanosheet composites are shown in Fig. S1b (Supporting information). The peak at 286 cm^{-1} attributes to the A_g vibration mode of $Cu_{12}Sb_4S_{13}$, and a blue shift phenomenon exists compared to $Cu_{12}Sb_4S_{13}$ thin film due to the intrinsic character of the tiny size for $Cu_{12}Sb_4S_{13}$ quantum dots [28]. In Raman spectrum of rGO nanosheet, two typical peaks appear at 1339 cm^{-1} and 1579 cm^{-1}, which originate from the D and G peaks of rGO, respectively [26,29]. The relative intensity (I_D/I_G) of 1.23 significantly proves that graphene oxide is partially reduced, which implies that a quite high percent of structure still exists between rGO and graphene [30]. Raman spectrum of $Cu_{12}Sb_4S_{13}$ quantum dots@rGO nanosheet composites shows the same vibration peak as compared with that of rGO nanosheet, in which I_D/I_G value of rGO nanosheet decreases to be 1.08, which confirms that rGO nanosheet in $Cu_{12}Sb_4S_{13}$ quantum dots@rGO nanosheet composites is further reduced during the formation of $Cu_{12}Sb_4S_{13}$ quantum dots@rGO nanosheet composites [26].

FESEM image of $Cu_{12}Sb_4S_{13}$ quantum dots@rGO nanosheet composites is shown in Fig. S2a (Supporting information), and it is obviously found that $Cu_{12}Sb_4S_{13}$ quantum dots are uniformly dispersed on the surface of rGO nanosheet. EDS mapping images of $Cu_{12}Sb_4S_{13}$ quantum dots@rGO nanosheet composites are shown in Figs. S2b–e (Supporting information), which reveals that all of C, Cu, Sb and S elements coexist in $Cu_{12}Sb_4S_{13}$ quantum dots@rGO nanosheet composites, and the dispersion of all elements is very uniform, which proves that $Cu_{12}Sb_4S_{13}$ quantum dots are uniformly dispersed on the surface of rGO nanosheet in $Cu_{12}Sb_4S_{13}$ quantum dots@rGO nanosheet composites.

TEM and HRTEM images of $Cu_{12}Sb_4S_{13}$ quantum dots/rGO composite are shown in Fig. 1. The inset in Fig. 1a is statistical histogram of the diameter distribution of $Cu_{12}Sb_4S_{13}$ quantum dots, which shows that the diameter of $Cu_{12}Sb_4S_{13}$ quantum dots is in a narrow range with the average diameter of 5.7 nm. From Fig. 1a, it can be easily found that rGO nanosheet in the composites remains thin and flat without substantial agglomeration, and $Cu_{12}Sb_4S_{13}$ quantum dots are uniformly distributed on the surface of rGO nanosheet and surrounded by several rGO nanosheet layers, which is mainly due to the fact that the exposed massive quantum dots may escape from agglomerating [26]. In Fig. 1b, the lattice fringes of rGO nanosheet are quite irregular, resulting from the many oxygen-containing groups distributed on rGO nanosheet. The inter-planar spacing of the lattice fringes is measured to be 0.1261 nm and 0.1370 nm, which correspond to (211) and (220) crystal planes of $Cu_{12}Sb_4S_{13}$ quantum dots, respectively. This is consistent with the XRD pattern in Fig. S1a. SAED pattern inset in Fig. 1b further proves the single crystal of $Cu_{12}Sb_4S_{13}$ quantum dots in $Cu_{12}Sb_4S_{13}$ quantum dots@rGO nanosheet composites.

The original resistances of $Cu_{12}Sb_4S_{13}$ quantum dots@rGO nanosheet composites, $Cu_{12}Sb_4S_{13}$ quantum dots and rGO nanosheet are shown in Figs. S3a–c (Supporting information), respectively. While their ammonia gas responses at room temperature under the humidity of 45% are measured, it can be generally revealed that the gas responses of all materials are dominated by the ammonia concentration, as shown in Figs. 2a and b. With the increasing of the ammonia concentration, the gas

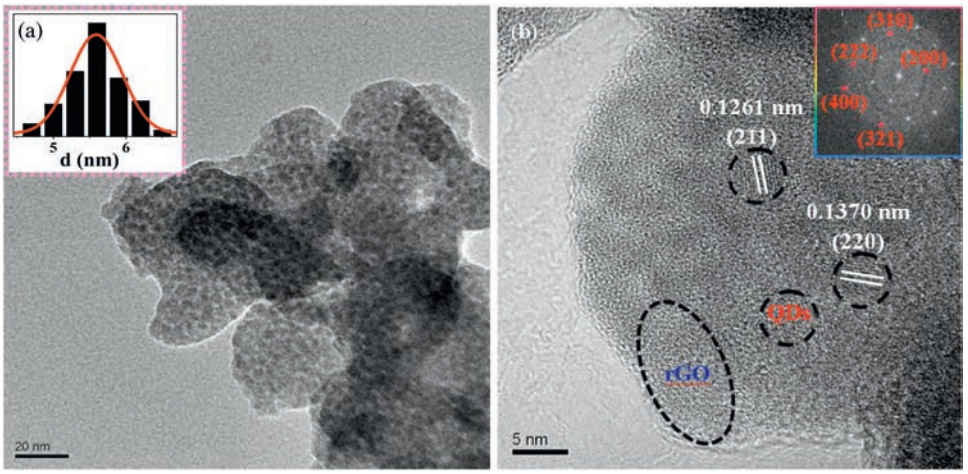

Fig. 1. (a) TEM image (inset is statistical histogram of the diameter distribution), (b) HRTEM image of $Cu_{12}Sb_4S_{13}$ quantum dots@rGO nanosheet composites.

responses of all gas sensors gradually increase. As the typical reductive gas for NH_3, the released electrons would inject into the composites due to the p-type behavior after the adsorption of NH_3 molecule, which would further induce to the resistance increasing [26–28]. Among them, $Cu_{12}Sb_4S_{13}$ quantum dots@rGO nanosheet composites possess a significant gas response with a low detection limit of 1 ppm compared to pure $Cu_{12}Sb_4S_{13}$ quantum dots and rGO nanosheet at room temperature. Especially, the gas response of $Cu_{12}Sb_4S_{13}$ quantum dots@rGO nanosheet composites to 250 ppm NH_3 is 1.389, which is nearly 1.28 times higher than that of pure $Cu_{12}Sb_4S_{13}$ quantum dots. Therefore, the composites of $Cu_{12}Sb_4S_{13}$ quantum dots with rGO nanosheet significantly improve the gas response in the NH_3 detection.

The response and recovery times are tested by repeating sensing process for two cycles with 50 ppm NH_3 and the average value is calculated in our case. Fig. 2c shows that the average response and recovery times of $Cu_{12}Sb_4S_{13}$ quantum dots@rGO nanosheet composites are 63 s and 133 s, respectively. It is considered that the large specific area and the massive active sites on the surfaces of $Cu_{12}Sb_4S_{13}$ quantum dots and rGO nanosheet may favor for the adsorption of ammonia gas molecules, which induces the relatively quick response [25,26].

Fig. 3a and Fig. S4a (Supporting information) show the gas response and the original resistance of $Cu_{12}Sb_4S_{13}$ quantum dots@rGO nanosheet composites towards 250 ppm NH_3 under different humidity in the range of 45%–80% at room temperature, respectively. It is found that the total loss of the gas response is only 4.08% in the humidity range from 45% to 80%, indicating the excellent stability of the gas response for $Cu_{12}Sb_4S_{13}$ quantum dots@rGO nanosheet composites to ammonia gas under different humidity. To investigate the influence of the surface state of $Cu_{12}Sb_4S_{13}$ quantum dots@rGO nanosheet composites on the gas response under various humidity, the compact $Cu_{12}Sb_4S_{13}$ quantum dots@rGO nanosheet composites film is fabricated for the measurement of water contact angle. The water contact angle (θ) is tested to be 80.78° as shown in Fig. S4b (Supporting information), which confirms the hydrophobicity characteristic of $Cu_{12}Sb_4S_{13}$ quantum dots@rGO nanosheet composites. The reason may lie in the fact that there are some residual organic ligands on the surface of $Cu_{12}Sb_4S_{13}$ quantum dots, which may prevent the absorption of water molecules in the air environment, leading to the excellent stability of $Cu_{12}Sb_4S_{13}$ quantum dots@rGO nanosheet composites under high humidity. The present work implies that $Cu_{12}Sb_4S_{13}$ quantum dots@rGO nanosheet composites may be considered as a good sensing material for ammonia detection under various humidity in reality.

In order to study the repeatability of gas sensing properties of $Cu_{12}Sb_4S_{13}$ quantum dots@rGO nanosheet composites, which are tested for four times towards 250 ppm NH_3 at room temperature and humidity of 45%, the gas response and the original resistance are shown in Fig. 3b and Fig. S4c (Supporting information). The results show that the gas response of $Cu_{12}Sb_4S_{13}$ quantum dots@rGO nanosheet composites after 4 cycles is quite stable, indicating a good repeatability of $Cu_{12}Sb_4S_{13}$ quantum dots@rGO nanosheet composites under humidity. Compared with some similar works, $Cu_{12}Sb_4S_{13}$ quantum dots@rGO nanosheet composites possess comparable or higher gas sensing performance. More interesting, $Cu_{12}Sb_4S_{13}$ quantum dots@rGO nanosheet composites show the quite excellent stability under high humidity, which is the best one as summarized in Table S1 (Supporting information) [31–34]. Especially, $Cu_{12}Sb_4S_{13}$ quantum dots@rGO nanosheet composites possess the excellent stability under high relative

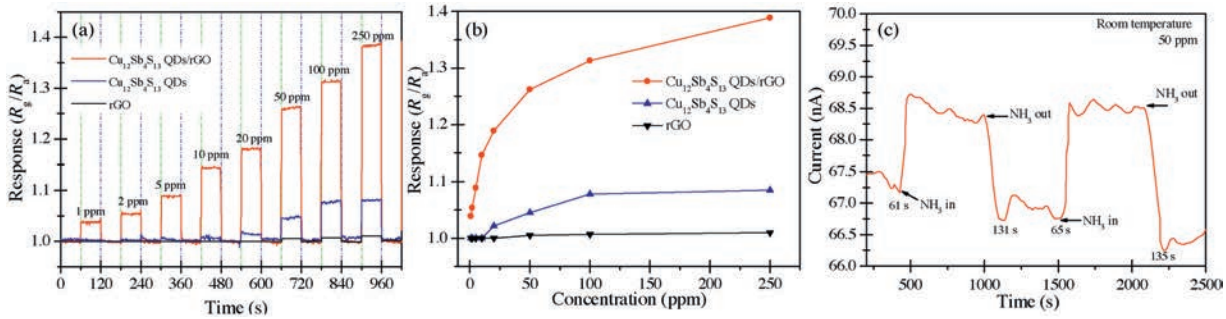

Fig. 2. Sensing performances of $Cu_{12}Sb_4S_{13}$ quantum dots@rGO nanosheet composites, $Cu_{12}Sb_4S_{13}$ quantum dots and rGO towards ammonia at room temperature: (a) The plots of response-time with various concentrations; (b) The plots of response-concentration of the target gas; (c) The response and recovery time.

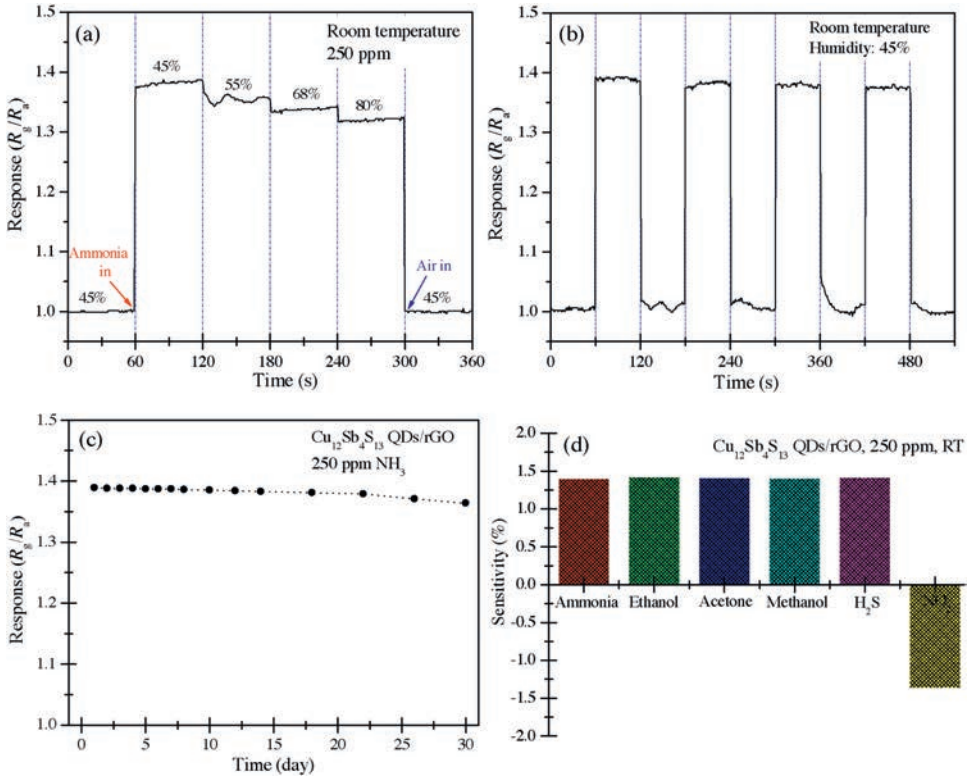

Fig. 3. The gas sensing performance of $Cu_{12}Sb_4S_{13}$ quantum dots@rGO nanosheet composites towards 250 ppm NH_3 at room temperature: (a) Gas responses under various humidity; (b) Gas responses after repeatability test at relative humidity of 45%; (c) The long-term stability and (d) selectivity of $Cu_{12}Sb_4S_{13}$ quantum dots@rGO nanosheet composites.

humidity compared with $CuSbS_2$ quantum dots@rGO nanosheet composites in our previous work [26]. The reason may be originated from the fact that the uniform dispersion of $Cu_{12}Sb_4S_{13}$ quantum dots on the surface of rGO nanosheet may enable a large surface to absorb the ammonia molecule, which is confirmed by the Brunauer-Emmett-Teller (BET) results. BET surface areas of $Cu_{12}Sb_4S_{13}$ quantum dots and $Cu_{12}Sb_4S_{13}$ quantum dots@rGO nanosheet composites are determined by N_2 adsorption using an ASAP-2020 surface area analyzer (Fig. S4d in Supporting information), which shows that $Cu_{12}Sb_4S_{13}$ quantum dots@rGO nanosheet composites possess higher specific surface areas (54.98 m^2/g) than that of $Cu_{12}Sb_4S_{13}$ quantum dots (36.74 m^2/g).

The long-term stability of the gas sensors is measured for 30 days, and a low loss of 2.7% for the gas response is observed in Fig. 3c, which further confirms the excellent stability of $Cu_{12}Sb_4S_{13}$ quantum dots@rGO nanosheet composites for the NH_3 detection. Various gases of ethanol, methanol, acetone, hydrogen sulfide and nitrogen dioxide with the concentration of 250 ppm are used to be mixed with 250 ppm ammonia, respectively, which are used as the detection gas for the gas selectivity of $Cu_{12}Sb_4S_{13}$ quantum dots@rGO nanosheet composites at room temperature and humidity of 45%, and the result is shown in Fig. 3d. It can be seen that the gas response has a slight change at various gases, which indicates that $Cu_{12}Sb_4S_{13}$ quantum dots@rGO nanosheet composites possess the superior selectivity towards ammonia.

DRIFT measurement is applied to investigate the functional groups and the possible reactions on the surface of $Cu_{12}Sb_4S_{13}$ quantum dots@rGO nanosheet composites, which is realized by the analysis of the vibration peaks during the adsorption and desorption processes of the target gas [26]. In our work, 20 sccm NH_3 (0.2%) with 1000 sccm N_2 is injected into the vacuum chamber after the N_2 decontamination during the adsorption process, during the desorption process the residual NH_3 on the composite surface is further swept by N_2 injection. Some substantial new peaks appear during the adsorption process as shown in Fig. 4a. The peak at 1016 cm^{-1}originates from N—H bending vibration, which proves that the coordinated ammonia bonds to Lewis acid sites [26]. The NH_4^+ on the Brønsted acidic sites may be proven by the existence of the peaks at 1396, 1463, 1693 and 1741 cm^{-1}, while the peaks at 3619, 3642 and 3679 cm^{-1} are assigned to be N—H vibration [26]. Moreover, some nitrate-based groups on the surface of $Cu_{12}Sb_4S_{13}$ quantum dots/rGO nanosheet composites also exist, including bridging nitrate species (1646 cm^{-1}), bidentate nitrate (1546 cm^{-1}), monodentate nitrate (1531 cm^{-1}) and nitrite species (1452 cm^{-1}), while the two peaks at 1835 and 1916 cm^{-1} confirm the existence of NO adsorption [26,35,36]. As a result, the above mentioned specific groups in Fig. 4a suggest that the active sites of $Cu_{12}Sb_4S_{13}$ quantum dots@rGO nanosheet composites for NH_3 adsorption may be Lewis and Brønsted acid sites [25,26].

As NO molecules are one of the possible productions during the NH_3 sensing process shown in Fig. 4a, which also evidently proves that the O_2^- ions originated from the pre-absorbed O_2 play a key effect. Moreover, NO molecules may further react with the O_2^- ions, inducing the formation of the nitrate-based groups as shown in Fig. 4a, such as nitrite species (1452 cm^{-1}), monodentate nitrate (1531 cm^{-1}), bidentate nitrate (1546 cm^{-1}) and bridging nitrate species (1646 cm^{-1}) [25,26]. The detail reaction process may be described in the following equations (Eqs. 1–4):

$$O_2(g) \rightarrow O_2(ads) \quad (1)$$

$$O_2(ads) + e^- \rightarrow O_2^- \ (T \leq 100^\circ C) \quad (2)$$

$$4NH_3 + 5O_2^- \rightarrow 4NO + 6H_2O + 5e^- \quad (3)$$

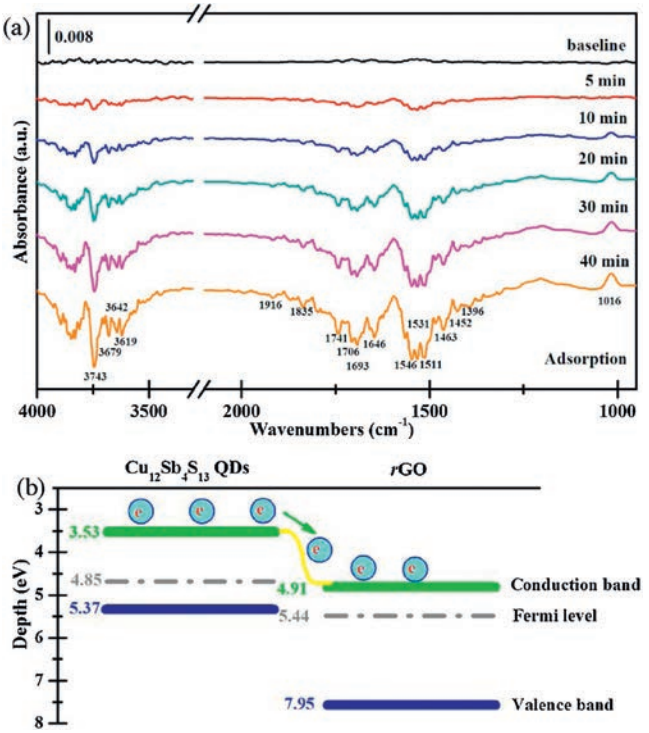

Fig. 4. (a) DRIFT spectra of $Cu_{12}Sb_4S_{13}$ quantum dots@rGO nanosheet composites at room temperature. (b) Schematic diagram of the bandgap structure for $Cu_{12}Sb_4S_{13}$ quantum dots@rGO nanosheet composites.

$$NO + O_2^- \rightarrow NO_3^- \quad (4)$$

As the size of quantum dots is comparable with the depth of the depletion layer, their mobile charge carriers are almost fully depleted, resulting in the fact that the depletion layer extends throughout the whole grain, which may eliminate the barrier for the charge transfer of inter-crystallites [25,26,37]. The above effect enables the excellent gas response of $Cu_{12}Sb_4S_{13}$ quantum dots@rGO nanosheet composites to NH_3 at room temperature, as $Cu_{12}Sb_4S_{13}$ quantum dots act as the surface modifiers and catalytically active centers for the ammonia adsorption [25,26].

Measured by UPS technique, the conduction band, Fermi level and valance band of 5.7 nm sized $Cu_{12}Sb_4S_{13}$ quantum dots are 3.53, 4.85 and 5.37 eV, respectively [38], while those of rGO nanosheet are 4.91, 5.44 and 7.95 eV, respectively [26]. Because of the different bandgap levels of $Cu_{12}Sb_4S_{13}$ quantum dots and rGO nanosheet, the electrons will transfer from the conduction band of $Cu_{12}Sb_4S_{13}$ quantum dots to the conduction band of rGO nanosheet, as shown in Fig. 4b [39,40]. rGO nanosheet mainly favors for the fast electron transfer in $Cu_{12}Sb_4S_{13}$ quantum dots@rGO nanosheet composites, therefore, the gas response of $Cu_{12}Sb_4S_{13}$ quantum dots@rGO nanosheet composites is significantly improved compared with pure $Cu_{12}Sb_4S_{13}$ quantum dots and rGO, which is consistent with the results in Fig. 2.

In conclusion, $Cu_{12}Sb_4S_{13}$ quantum dots@rGO nanosheet composites are prepared by solvent thermal method. Gas sensing response of $Cu_{12}Sb_4S_{13}$ quantum dots@rGO nanosheet composites towards ammonia at room temperature is greatly enhanced compared with pure $Cu_{12}Sb_4S_{13}$ quantum dots and rGO nanosheet with a low detection limit of 1 ppm. Humidity test proves that $Cu_{12}Sb_4S_{13}$ quantum dots@rGO nanosheet composites possess an excellent stability with the total loss of 4.08% in the humidity range from 45% to 80%, and the gas response of $Cu_{12}Sb_4S_{13}$ quantum dots@rGO nanosheet composites after 4 cycles at the humidity of 45% is quite stable, which is related with the intrinsic hydrophobicity characteristic of $Cu_{12}Sb_4S_{13}$ quantum dots. The good selectivity and the stability in a long term prove that $Cu_{12}Sb_4S_{13}$ quantum dots@rGO nanosheet composites may be a good candidate for the practical ammonia detection. The highly sensitive nature of $Cu_{12}Sb_4S_{13}$ quantum dots@rGO nanosheet composites may be related with the enhanced gas absorption ability of $Cu_{12}Sb_4S_{13}$ quantum dots as well as the fast charge transport from $Cu_{12}Sb_4S_{13}$ quantum dots to rGO nanosheet due to the well-combined interfaces of $Cu_{12}Sb_4S_{13}$ quantum dots@rGO nanosheet composites.

Declaration of competing interest

The authors declare that they have no known competing financial interests or personal relationships that could have appeared to influence the work reported in this paper.

Acknowledgments

This work was supported by the National Natural Science Foundation of China (No. 11674258), the 111 Project (No. B18038), Key projects of Natural Science Foundation of Hubei Province (No. 2019CFA044), Applied Basic Research Program of Wuhan (No. 2018010401011278), Science and Technology Innovation Program of Hubei Province (No. 2018BKJ005), Natural Science Foundation of Hunan Province, China (No. 2018JJ3527) and Students Innovation and Entrepreneurship Training Program (No. 20181049721003). Thanks for the measurements supporting from Centre for Materials Research and Analysis at Wuhan University of Technology (WUT).

Appendix A. Supplementary data

Supplementary material related to this article can be found, in the online version, at doi:https://doi.org/10.1016/j.cclet.2019.12.030.

References

[1] J. Bai, B.X. Zhou, Chem. Rev. 114 (2014) 10131–10176.
[2] Y.K. Li, J.J. Zhang, Z.J. Bian, et al., Chin. Chem. Lett. 27 (2016) 518–522.
[3] L. Liu, X.M. Yu, B. Zhang, S.X. Meng, Y.Q. Feng, Chin. Chem. Lett. 28 (2017) 765–770.
[4] B. Timmer, W. Olthuis, A. Van Den Berg, Sens. Actuator. B -Chem. 107 (2005) 666–677.
[5] Y. Li, X. Wang, C.Y. Xing, et al., Chin. Chem. Lett. 30 (2019) 1440–1444.
[6] W.C. Wang, F.Q. Liu, B. Wang, Y.D. Wang, Chin. Chem. Lett. 30 (2019) 1261–1265.
[7] V. Modafferi, G. Panzera, A. Donato, et al., Sens. Actuator. B -Chem. 163 (2012) 61–68.
[8] K. Xu, N. Li, D.W. Zeng, et al., ACS Appl. Mater. Interfaces 7 (2015) 11359–11368.
[9] J. Wang, P. Yang, X.W. Wei, ACS Appl. Mater. Interfaces 7 (2015) 3816–3824.
[10] A.K. Prasad, D.J. Kubinski, P.I. Gouma, Sens. Actuator. B -Chem. 93 (2003) 25–30.
[11] Q. Zhang, H. Zhang, M.K. Xu, Z.R. Shen, Q. Wei, Chin. Chem. Lett. 30 (2019) 1261–1265.
[12] H. Liu, M. Li, O. Voznyy, et al., Adv. Mater. 26 (2014) 2718–2724.
[13] M. Epifani, E. Comini, R. Díaz, et al., ACS Appl. Mater. Interfaces 6 (2014) 16808–16816.
[14] A. Rothschild, Y. Komem, J. Appl. Phys. 95 (2004) 6374–6380.
[15] B.H. Zhang, M. Li, Z.L. Song, et al., Sens. Actuators B -Chem. 249 (2017) 558–563.
[16] J.P. Du, R.H. Zhao, Y.J. Xie, J.P. Li, Appl. Surf. Sci. 346 (2015) 256–262.
[17] M. Li, J.T. Luo, C. Fu, et al., Sens. Actuator. B -Chem. 256 (2018) 1045–1056.
[18] L. Wang, B. Yang, Z. Xia, et al., Sol. Energy Mater. Sol. Cells 144 (2016) 33–39.
[19] K.Q. Chen, J. Zhou, W. Chen, et al., Part. Part. Syst. Charact. 32 (2015) 999–1005.
[20] K.Q. Chen, J. Zhou, W. Chen, et al., Nanoscale 8 (2016) 5146–5152.
[21] M. Thripuranthaka, N. Sharma, T. Das, et al., Adv. Mater. Interfaces 5 (2018) 1701492.
[22] Z. Song, Z. Wei, B. Wang, et al., Chem. Mater. 28 (2016) 1205–1212.
[23] L. Zhou, F. Shen, X. Tian, et al., Nanoscale 5 (2013) 1564–1569.
[24] R.K. Mishra, S.B. Upadhyay, A. Kushwaha, et al., Nanoscale 7 (2015) 11971–11979.
[25] Y.L. Liu, H.R. Wang, S. Yang, et al., Sens. Actuator. B -Chem. 255 (2018) 2979–2987.
[26] Y.L. Liu, H.R. Wang, K.Q. Chen, et al., ACS Appl. Mater. Interfaces 11 (2019) 9573–9588.
[27] K.Q. Chen, J. Zhou, W. Chen, et al., Nanoscale 9 (2017) 12470–12478.
[28] Y.L. Liu, L.L. Wang, H.R. Wang, et al., Sens. Actuator. B -Chem. 236 (2016) 529–536.
[29] L. Zhang, Y. Li, X. Li, et al., Nano Energy 28 (2016) 135–142.

[30] L. Dou, H. Zhang, J. Mater. Chem. A 4 (2016) 18990–19002.
[31] G. Lee, M.R. Jo, K. Zhang, Y. Kang, J. Mater. Chem. A 5 (2017) 3683–3690.
[32] R. Ghosh, A. Midya, S. Santra, S.K. Ray, P.K. Guha, ACS Appl. Mater. Interfaces 5 (2013) 7599–7603.
[33] W. Chen, F. Li, P.C. Ooi, et al., Sens. Actuator. B -Chem. 222 (2016) 763–768.
[34] J.N. Gavgani, A. Hasani, M. Nouri, M. Mahyari, A. Salehi, Sens. Actuator. B -Chem. 229 (2016) 239–248.
[35] J. Fan, P. Ning, Z. Song, et al., Chem. Eng. J. 334 (2018) 855–863.
[36] Y. Chen, Z. Zhang, L. Liu, L. Mi, X. Wang, Appl. Surf. Sci. 366 (2016) 139–147.
[37] A. Rothschild, Y. Komem, J. Appl. Phys. 95 (2004) 6374–6380.
[38] Y.L. Liu, Q. Chen, A.H. Mei, et al., Sustain. Energy Fuels 3 (2019) 831–840.
[39] J. Zhang, X.H. Liu, G. Neri, N. Pinna, Adv. Mater. 28 (2016) 795–831.
[40] J.H. Lee, A. Katoch, S.W. Choi, et al., ACS Appl. Mater. Interfaces 7 (2015) 3101–3109.